

# MULTI-IMAGE MATCHING IN OBJECT SPACE USING AIRBORNE CCD-LINESCANNER IMAGERY

Martin SCHLÜTER

Bundesamt für Kartographie und Geodäsie  
Richard-Strauss-Allee 11, D-60598 Frankfurt am Main, Germany  
Phone: +49-69-6333-306  
martin.schlueter@ifag.de

Working Group III/2, International Society of Photogrammetry and Remote Sensing,  
19th ISPRS Congress, Amsterdam, The Netherlands, July 2000

**KEY WORDS:** Surface reconstruction, Image matching in object space, High-resolution images, DTM / DEM / DSM, Facets Stereo Vision.

## ABSTRACT

An object space-based strategy for simultaneous multi-image matching of airborne stereoscopic CCD-linescanner imagery is introduced. The goal of the presented algorithmic solution is to improve and to simplify the automated processing of large-scale aerial linescanner imagery.

A very straightforward strategy can be formulated using image pyramids directly calculated from the raw, unrectified linescanner imagery. It is evaluated whether the impacts of the approximations thereto attached can be accepted for the estimation of the intermediate start values of the geometric surface description. For this purpose an image strip taken by the digital photogrammetric three-line scanning camera DPA (=Digital Photogrammetric Assembly) is analysed and the results are discussed. Finally, at the original image resolution, the suggested approach of multi-image matching in object space offers a mathematically strict solution for multi-image matching of airborne CCD-linescanner imagery.

## 1 PHOTOGAMMETRIC PROCESSING OF AIRBORNE CCD-LINESCANNER IMAGERY AT THE BKG

The working fields of the BKG (=Federal Office for Cartography and Geodesy) tend to shift towards larger scales of its main products, both maps and digital cartographic databases. Apart from the fact that this might be considered as a global trend, at the BKG this progress is actually driven by relatively new tasks concerning the collection, harmonisation, provision and administration of ATKIS (=Authoritative Topographic-Cartographic Information System) data at federal level. ATKIS constitutes, roughly outlined, the digital representation of the topographic maps at the scale 1 : 25 000, its data was captured and is maintained by the survey administrations of the sixteen federal states (Laender) of Germany. To meet the requirements of the automated acquisition of geodata at this scale, satellite imagery is and will often not be sufficient (Englisch and Heipke, 1998). Against this, the digital photogrammetric camera seems to be a very interesting tool for the near future: ground resolutions of about  $10 \times 10 \text{ cm}^2$  to  $50 \times 50 \text{ cm}^2$  can easily be achieved while stereo and multispectral exposures are possible. Furtheron, the management of an airborne sensor can be done much more flexibly than that of a satellite platform; thus, typical problems of satellite imagery like occlusions caused by clouds, inappropriate solar angles, improper exposure times due to rigid exposure cycles, etc. can and will be handled in a more cost-effective way. Against the scanning of analogue images the digital camera offers a high-grade improved signal-to-noise ratio of the grey values. Both automatic recognition algorithms and automatic surface reconstruction will profit from this feature.

In this regard the BKG is interested in obtaining practical expertise concerning the processing of airborne CCD-line imagery, since this seems to be one of the most promising concepts for the digital photogrammetric camera, (Hofmann et al., 1993), (Albertz, 1998), (Sandau et al., 1999). Recently finished works at the BKG concentrated on the realisation of a processing chain starting from raw image data including the exterior orientations and finally entering classical digital photogrammetric workstations like the HELAVA-DPW 770. The goal consisted in obtaining performance of well-founded quality controls for existing and newcoming digital cameras (Schlüter, 1999a). Central and in our opinion particularly open questions are the evaluation of the overall geometric accuracy of a complete camera system, the integration of DGPS-, IME- and tie point measurements within a bundle adjustment approach ('are tiepoints necessary?'), and the possibilities and limitations of self-calibration using a photogrammetric bundle adjustment approach – as it was successfully carried out for space applications like IRS-1C (Jacobsen, 1997) or MOMS-02P (Kornus et al., 1998).

---

The project described in this publication was promoted by funds of the Bundesministerium für Bildung, Wissenschaft, Forschung und Technologie (Federal Ministry for Education, Cultural Affairs, Research and Technology) under the registration number 50 EE 9604. The author assumes responsibility for the contents of the present publication.

First experiences were gathered with data from the camera prototype DPA (=Digital Photogrammetric Assembly) by DaimlerChrysler Aerospace, cf. fig. 1. The above-mentioned processing chain was successfully tested. Although the aspired accuracy of below  $\pm 1$  pixel on the ground was not reached – residual parallaxes of about  $\pm 3$  pixels still remained – it was possible to denominate and to clearly rate the accuracy limiting factors, (Haala et al., 1998), (Schlüter, 2000). (The main one was proved to be an error of a hardware connection of the IME and has been fixed in the meantime.) Our conclusion is that an operational digital aerial camera system should offer the possibility of integrating DGPS-, IME-, control point and tie point data within a bundle adjustment approach (at least to obtain some degrees of redundancy), and should offer the option of a self-calibration performance if required. Under this general conditions it should be easy to reach an accuracy near or below one pixel as was reported recently for a similar camera system (Wewel and Brand, 1999).

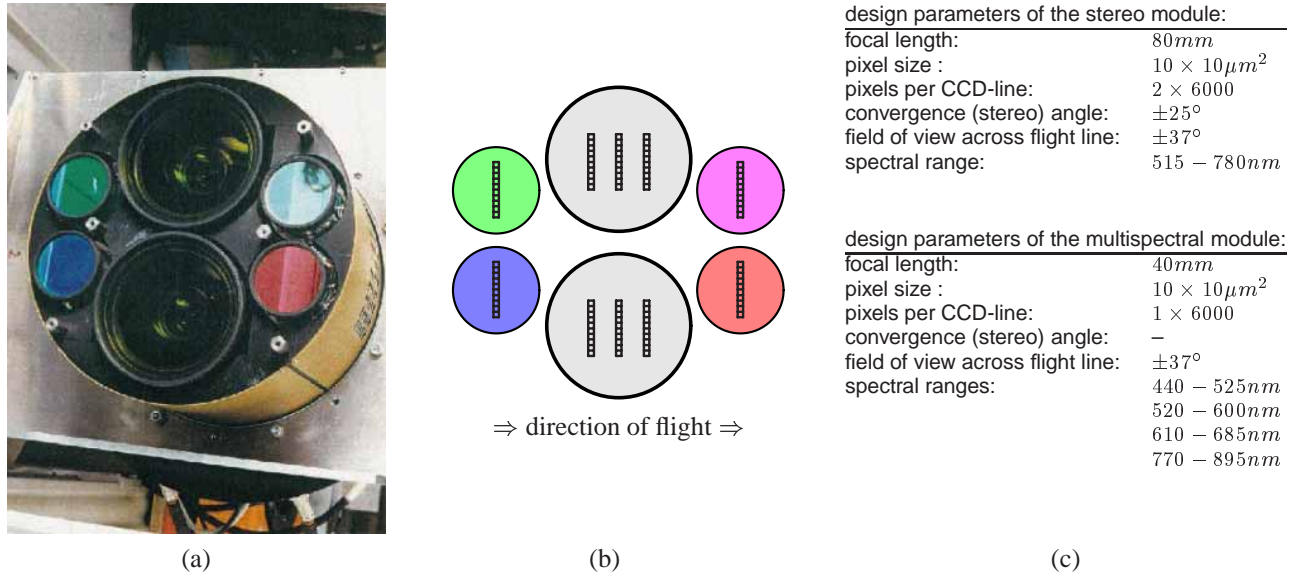


Figure 1: Camera design of DPA, (Angermaier et al., 1998). (a): Photograph from laboratory. (b): Arrangement of optics and CCD-lines. (c): Selected camera parameters.

In the following, the focus will be on an appropriate strategy for multi-image matching of CCD-linescanner images (but not on the restitution of the orientations). Availability of proper numerical values for the interior and exterior orientations is presumed. The concept of facets stereo vision due to (Wrobel, 1987) is applied and discussed with respect to some typical characteristics of airborne CCD-linescanner data. For the calculation of initial values for the surface geometry, which only have intermediate character during the hierarchical reconstruction procedure, the use of image pyramids obtained directly from the unrectified raw image is proposed. This offers a numerically smart strategy while achieving a mathematically strict final solution. A selected DPA image strip is used to empirically evaluate this way of proceeding.

## 2 APPLICATION OF FACETS STEREO VISION TO CCD-LINESCANNER IMAGERY

Fig. 2 introduces the concepts of image matching in image space and in object space, respectively. Image matching in image space adapted to data from airborne CCD-linescanners often requires at least locally rectified image windows. This has the consequence that after the rectification step the simple relation between raw pixel coordinates and interior and exterior orientation is lost and has to be reestablished by an iterative procedure (Haala et al., 1998). This strategy might be acceptable, if only a few points have to be determined, for instance for tie point matching during the phase of orientation. It seems to be not economical for surface reconstruction with the aim a high point density of the resulting surface description in object space. Whereas image-to-image-matching is a little long winded with respect to airborne linescanner imagery, the object-orientated approach looks much more straightforward: A (raw) pixel grey value is projected into object space taking all geometric information directly into account: The pixels' position in image space due to its interior orientation as well as its exterior orientation according to its time stamp. It is not important how much the orientations differ from scanline to scanline within the raw data, since most of the processing concerning the surface reconstruction itself is done on the ground (and reprojection of every grid point is not necessary).

Lets now have a closer look at the object space-based proceeding: A pixel of a CDD-linescanner flight mission can be identified by its position (row and column within the raw image) and the specification of the CCD-line and the flight strip. Usually, this is equivalent to the denotation of the pixel by its position  $(x', y')$  in the (in case of DPA: fictitious) image plane according to the interior orientation parameters of the CCD-line and the time stamp  $t$  of the moment of exposure.  $t$  offers the link to the varying parameters of the exterior orientation, so the centre of projection within a flight strip is in the following denoted by  $\mathbf{X}'_0(t) = (X'_0(t), Y'_0(t), Z'_0(t))$ . In this sense, the image pixel grey value is

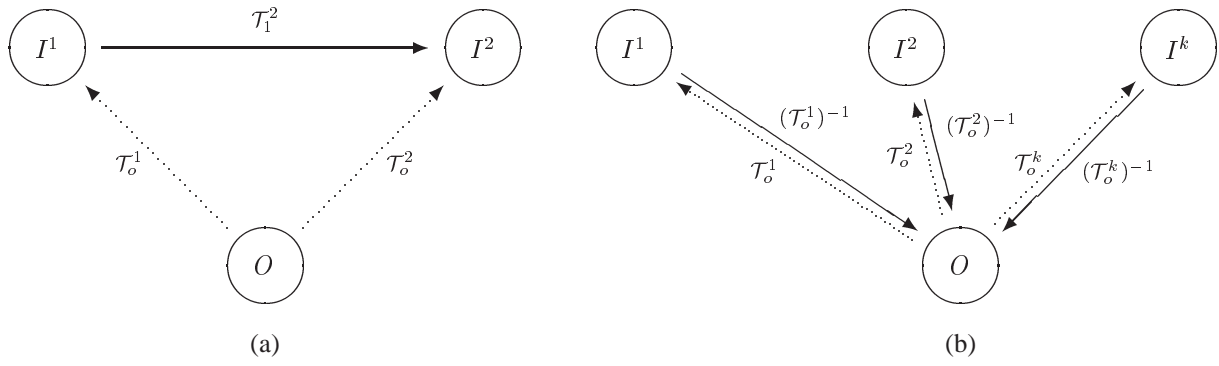


Figure 2: Image space-based and object space-based image matching, following (Lang and Förstner, 1995). The images  $I^i$ ,  $i = 1, 2, \dots, k$  of object space  $O$  result from the transformations  $\mathcal{T}_o^i$ . (a): Reconstruction of object space  $O$  by the estimation of  $\mathcal{T}_1^2$  in image space. (b): Reconstruction of  $O$  by the inversion of  $\mathcal{T}_o^i$  in object space.

referenced by  $g^i(x^i, y^i, t)$ . As mentioned above, the proceeding of image matching in object space can be characterized, roughly and colorfully speaking, by the following: Interpret each pixel grey value as an observation in the sense of a least squares' estimation, project it to object space, according to its interior and exterior orientation, and formulate the observation equation of each image pixel grey value with respect to the unknown parameters in objects space. The unknown parameters are mainly the parameters of the geometric surface model and the parameters of the surface grey values in object space (usually the orthoimage), but also some radiometric parameters have to be introduced. Last but not least, add some regularization equations, (Wrobel et al., 1992), solve the resulting normal equations and calculate even standard deviations of the unknowns if requested.

The correspondence condition between the image pixel grey value  $g^i(x^i, y^i, t)$  and the surface grey value  $G(X, Y)$  in object space is the basic starting point for the observation equation, cf. fig. 3, with the residual  $v_g(x^i, y^i, t)$  of the image grey value and the radiometric parameters  $h_1^i$  and  $h_2^i$  (defined with local validity within each image strip):

$$\begin{aligned}
 & (g^i(x^i, y^i, t) + v_g(x^i, y^i, t)) \cdot h_2^i + h_1^i & (1) \\
 & = G(X, Y) \\
 & = G^\circ(X^\circ, Y^\circ) + dG^\circ(X^\circ, Y^\circ) + \left( \frac{\partial G^\circ(X^\circ, Y^\circ)}{\partial X} \left( \frac{X^\circ - X_0^i(t)}{Z^\circ - Z_0^i(t)} \right) + \frac{\partial G^\circ(Y^\circ, Y^\circ)}{\partial Y} \left( \frac{Y^\circ - Y_0^i(t)}{Z^\circ - Z_0^i(t)} \right) \right) dZ^\circ(X^\circ, Y^\circ)
 \end{aligned}$$

The surface reconstruction process is started from a coarse approximation of the geometric surface  $Z^\circ(X, Y)$  and its corresponding orthoimage  $G^\circ(X, Y)$ . The ray of the image pixel  $(x^i, y^i, t)$ , defined by the exterior orientation with the corresponding time stamp, intersects the surface at  $(X^\circ, Y^\circ, Z^\circ)$ , for which a linear Taylor series expansion is set up to correct  $G^\circ$  by  $dG^\circ$  and  $Z^\circ$  by  $dZ^\circ$ . To build the final (linearized) observation equation,  $dG^\circ$  and  $dZ^\circ$  have to be replaced from their respective models. A variety of models for the surface itself as well as for the surface grey values have been yet well-tried, for instance bilinear interpolation (Weissensee, 1992), cubic convolution, wavelets (Tsay, 1996) and splines with full 3-d capability (Schlüter, 1999b). Questions of surface modeling will not be discussed in this section, because the choice of an appropriate surface model can be kept absolutely independent from the sensor design of the digital photogrammetric camera, as long as the *direct pixel transfer* as described above is applied. This is the main distinction against previously published suggestions for the application of object space-based image matching to satellite imagery using the indirect pixel transfer (Diehl and Heipke, 1992).

To reach a high degree of independence concerning the initial heights  $Z^\circ(X, Y)$  required in object space, which describe the approximate run of the surface, one usually falls back on multigrid techniques in object space resp. image pyramids in image space. This has been found a reasonable procedure for both terrestrial and aerial imagery, if the images are scanned at sufficiently high resolution, (Schlüter and Kempa, 1993), (Schlüter and Wrobel, 1996). From a theoretical point of view, the adoption of image pyramid techniques for unrectified raw linescanner images seems to be a critical point with respect to the application of facets stereo vision. Unlike working with image data at its original resolution, where all available geometric information is taken strictly into account, standard low-pass filtering during the creation of image pyramids from the unrectified image data is based on the assumption of regularly spaced and neighbored pixels. But this assumption is usually not valid from scanline to scanline of raw airborne linescanner data, because of the typically irregular and high-frequent motions of the camera caused by the airplane. Since only the calculation of *intermediate* approximative values  $Z^\circ(X, Y)$  is concerned – the final result is not affected as long as the radius of convergence, which is at least two or three pixels, is not exceeded! – an exemplary and empirical consideration given in the following section will show, whether the (intermediately) occurring error budget can be tolerated or not.

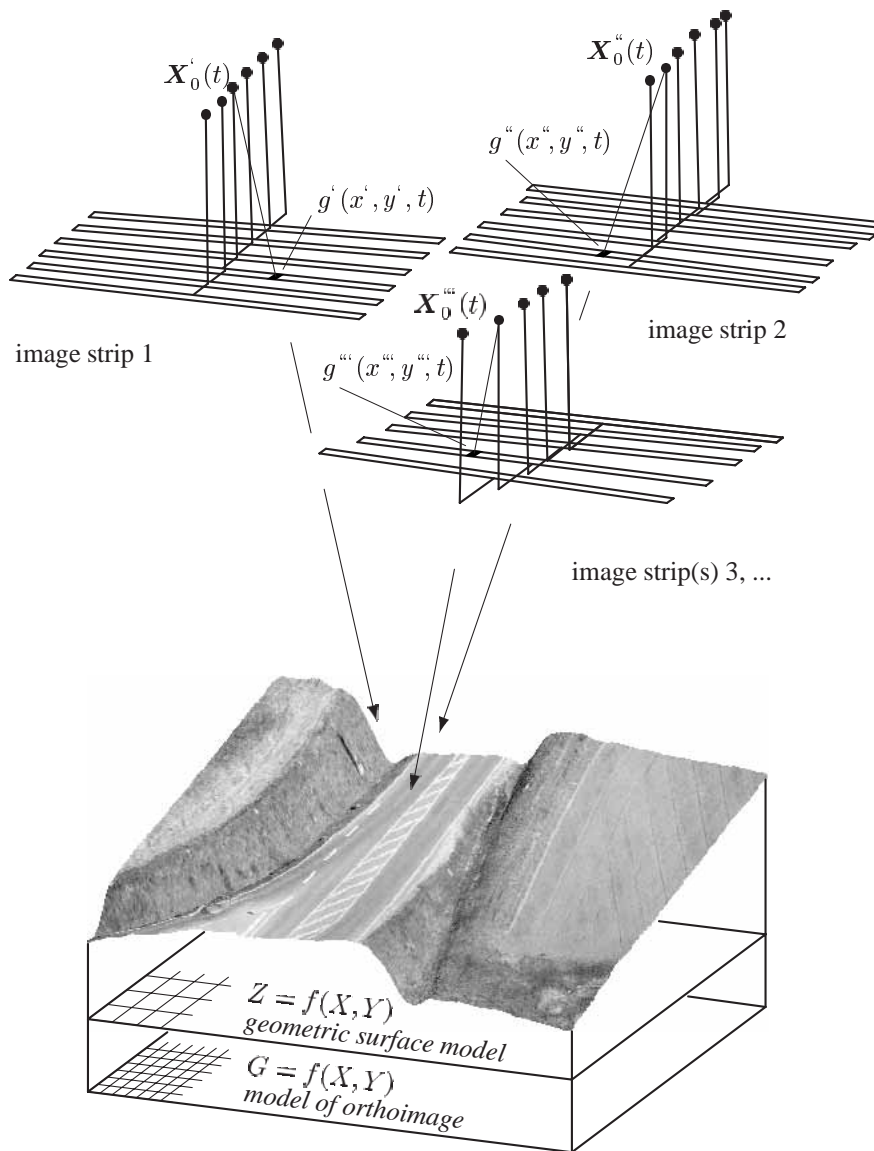


Figure 3: Multi-image matching in object space with CCD-linescanner data. The projection rays from three image pixels are outlined. The parameters of the surface model  $Z = f(X, Y)$  and the orthoimage  $G = f(X, Y)$  are estimated by least squares' adjustment. The point density of the orthoimage grid is typically finer than the point density of the geometry grid.

### 3 THE USE OF IMAGE PYRAMIDS CALCULATED FROM UNRECTIFIED LINESCANNER IMAGERY

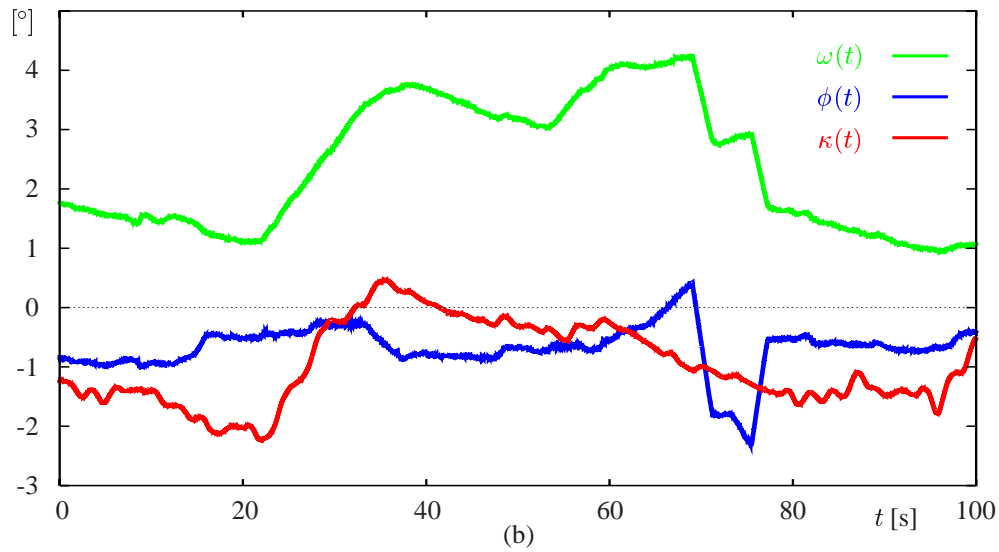
How do the geometrically irregular adjacencies of the pixel scanlines of raw CCD-linescanner imagery affect the hierarchical surface reconstruction procedure if the image pyramids are calculated directly from the unrectified raw data? To answer this question by a worst-case assessment, we choose one of the DPA image strips for an empirical test, cf. fig. 4. The imagery was taken from a flight altitude of about  $3000m$  above ground with a mean pixel size of  $\approx 37.5 \times 37.5cm^2$  on the ground, the total strip width is about  $4km$  on the ground. In the central image area you will find the city of *Hofheim am Taunus*. This image strip was chosen because it shows two extreme changes of the orientation parameters at  $t_1 = 70s$  and  $t_2 = 77s$  besides the typically small and high-frequent changes, so a wide range of values is covered by this exemplary data, cf. fig. 4(b). You may recognize the corresponding locations of the extreme changes of the orientation parameters when examining the margin of the rectified image, fig. 4(c).

The image pyramids in this paper were built on the basis of the approximation of an ideal low-pass filter according to the bottom line in table 1, which in theory fulfills the needs of an 'ideal'  $13 \times 13$  low-pass filter mask (Meer et al., 1987); but in practice only the computational costs of a  $7 \times 7$  mask arise due to zero columns and rows. In our experience this is the maximum effort one is usually willing to expend for the calculation of an image pyramid. For many applications a smaller filter mask might be considered to be sufficient. But the goal of this choice was to aspire something like a 'worst-case scenario' with respect to the creation of image pyramids from raw linescanner data, where the largest mask size seems

⇒ direction of flight ⇒



(a)



(b)



(c)

Figure 4: Geometric rectification of a complete DPA flight strip ('Frankfurt-West 9A'). (a): Raw image strip, 12 000 × 24 000 pixels. (b): Rotations  $\omega(t)$ ,  $\phi(t)$ ,  $\kappa(t)$  for each image scanline. (c): Geometrically rectified image strip.

to be the most dangerous one – although the differences between the listed filters should not be overestimated according to the low values at the border of the filter masks. Of course the renunciation of low-pass filtering is always the worst solution, since it causes aliasing effects, which are clearly visible at first glance by optical inspection of the exemplary data and are not acceptable for accurate and robust image matching at the higher levels of the image pyramid.

size of filter mask	low-pass filter kernel = $\ell^\top \cdot \ell$	relative computation time
$3 \times 3$	$\ell = \frac{1}{4}(1, 2, 1)$	1
$5 \times 5$	$\ell = \frac{1}{25}(1, 4, 6, 4, 1)$	2.78
$\Rightarrow 11 \times 11$	$\ell = \frac{1}{1000}(51, 0, -87, 0, 298, 475, 298, 0, -87, 0, 51)$	5.44 $\leftarrow$

Table 1: Several low-pass filter kernels for the creation of image pyramids (Kaiser et al., 1992).

To obtain an overview of the error of budget, which results from building the image pyramids directly from the unrectified raw imagery, two images derived from the complete image strip shown in fig. 4 are compared at the 2<sup>nd</sup> pyramid level in the following, both being rectified with respect to a horizontal plane in object space. The first one is created in the approximative way like it will be used by the fast and straightforward strategy for multi-image matching: First, the image pyramid is created and afterwards the image at 2<sup>nd</sup> pyramid level is rectified by projecting the pixels to object space according to their orientation parameters. This image is labelled 'post-rectified' at 2<sup>nd</sup> level. The second image for the comparison is created in a theoretically more appropriate, but – if applied with respect to the hierarchical surface reconstruction we have in mind – also much more complicated way: First, the original raw image is rectified. Then, within the rectified image, the pixels are geometrically regularly spaced and neighboured. This allows appropriate application of standard low-pass filtering. The image pyramid is built afterwards, the resulting image at the 2<sup>nd</sup> level is called 'pre-rectified' in the following. If we now compare the pre- and post-rectified images, the resulting error budget will contain primary the differences we are interested in to know. Secondary, there might be some additional differences due to the interpolation steps performed during the two different ways of rectification, which both cause some additional low-pass filtering. This is accepted, since we are trying to assess a worst-case scenario, as mentioned above.

The direct comparison of the pre- and post-rectified images shows that the post-rectified image seems to be a little over-smoothed. According to this observation the variance of all its grey values is a little reduced compared to the one of the pre-rectified image at 2<sup>nd</sup> level. But in both cases aliasing is avoided successfully. The order of the geometric differences, which occur between the pre- and post-rectified images, is of main interest. These differences are evaluated for the complete image strip with the program SIR (=subpixel image registration), which was designed to reach geometric accuracies up to the tenth part of a pixel (Boochs, 2000). SIR works on the basis of a regular grid in the master image and is well-suited for the detection of the small geometric differences between pre- and postrectified images. Overall, about 640 000 difference vectors have been calculated using a window size as small as possible for the registration procedure. 99.7% of the geometric differences are within a range of  $\pm$  a fourth pixel at 2<sup>nd</sup> level, absolute differences greater than half of a pixel do not appear. Small local systematics are typical, which seem to be fully independent from the low-frequent changes of the orientation parameters, cf. fig. 5. Fig. 5(c) shows the geometric difference vectors corresponding to the exemplary window of an image area with extremely changing orientation parameters. It is remarkable that the geometric differences in flight direction are about 20–30% larger than in the direction of the sensor lines. This means, that mainly the X-parallaxes (= small intermediate height errors) are affected by the appearing error characteristics, but that the dis-

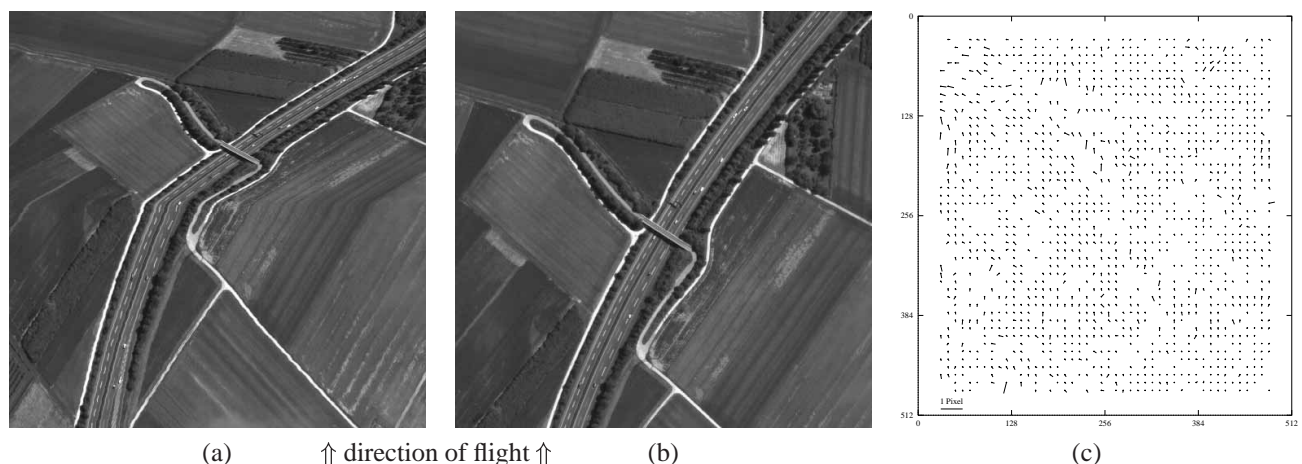


Figure 5: DPA image window (road B40 near *Hattersheim am Main*). (a): Raw image window ( $1024 \times 1024$  pixels). (b): Rectified image, 2<sup>nd</sup> pyramid level ( $512 \times 512$  pixels); (=pre- or postrectified image, both look very similar in print) (c): Geometric differences between the pre- and postrectified images at 2<sup>nd</sup> pyramid level.

turbances of the epipolar constraint (= errors caused by Y-parallaxes) within one flight strip are secondary. Altogether, the absolute values of the observed geometric differences are small to such a degree, that both the danger of trespassing the radius of convergence during the multigrid reconstruction process and the occurrence of matching failures due to large Y-parallaxes can be neglected.

#### 4 CONCLUSIONS

The exemplary evaluations of the last section show that it is possible to base the photogrammetric surface reconstruction in object space on image pyramids which are calculated directly from the raw CCD-linescanner imagery without any pre-rectification. This leads to a very straightforward and computation time-saving concept for surface reconstruction, since consequently only the direct projection of pixels into object space is required, and the long winded backprojection into the irregular pixel-topology of image space can be completely avoided.

Furthermore, the concept of object space-based image matching allows simultaneous matching of more than two image strips in a very simple way. Multi-image matching offers higher degrees of accuracy and robustness as previous investigations based on classical aerial imagery have shown (Schlüter and Wrobel, 1996). The first step would consist in the integration of the grey value information of all three CCD lines of DPA, for instance. But in general it is not essential whether the image strips for a simultaneous surface reconstruction are taken all from the same or additionally from adjacent or crossing flight strips, as long as all the orientation parameters are valid within the global reference frame of the photo flight. Following this multi-image strategy in an exhaustive way, one might also take advantage towards automatic digital surface reconstruction of difficult areas like built-up scenes. In the past, investigations based on scanned large-scale aerial images have shown that simultaneous use of four or better more images can significantly improve the matching results. The basic requirement is, that the reconstruction algorithm can benefit from the complete visible information, which is available within each of the participating images, even if vertical (or overhanging) parts of buildings are pictured. Fig. 6 illustrates the reason: Within one image strip, many vertical walls of the buildings are visible, but usually only in a monoscopic but not in a stereoscopic way. Adjacent flight strips with a high overlap can offer the stereoscopic information, which can be used by sophisticated approaches for multi-image matching. Especially for built-up scenes, the integration of a general 3-d surface model in object space, which handles automatically arbitrary surfaces in  $\mathbb{R}^3$ , has proven its superiority to common formulations based on 2.5-d surface models like  $Z=f(X,Y)$ , cf. (Schlüter, 1998).

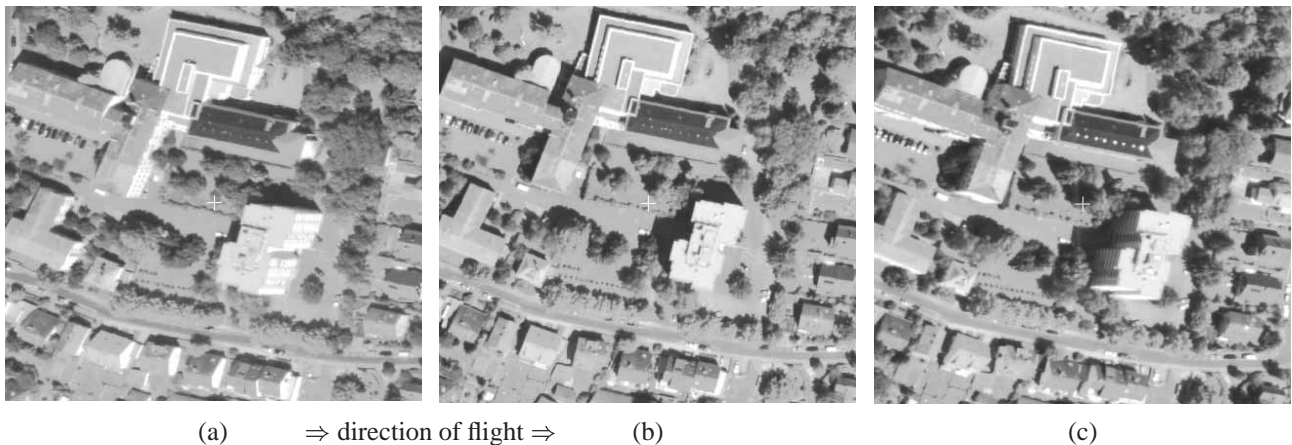


Figure 6: DPA imagery of a built-up scene. (a): Backward view. (b): Nadir view. (c): Forward view.

Due to the above-mentioned deficiencies of the absolute exterior orientations it was actually not possible to explore the matching accuracies for the presented approach. They should be investigated with imagery of the now modified DPA or by means of another digital photogrammetric camera like HRSC or LH's new airborne digital sensor in the near future.

#### REFERENCES

- Albertz, J., 1998. The geometric restitution of line scanner imagery – three decades of technical development. In: Festschrift Univ.-Prof. Dr.-Ing. Dr.h.c.mult. Gottfried Konecny zur Emeritierung, Wissenschaftliche Arbeiten der Fachrichtung Vermessungswesen der Universität Hannover, Vol. 227, pp. 25–34.
- Angermaier, A., Hockling, T., Klein, W. and Müller, F., 1998. Digitale Photogrammetrie-Ausstattung (DPA). Schlußbericht FE IV 1 - T/F41G/V0018/24257, Daimler-Benz Aerospace, LFK GmbH, München.
- Boochs, F., 2000. Ein Verfahren zur präzisen gegenseitigen geometrischen Einpassung von Multispektralbildern. In: J. Albertz (ed.), Photogrammetrie und Fernerkundung: Neue Sensoren – Neue Anwendungen; Vorträge 19. Wissenschaftlich-Technische Jahrestagung der DGPF, 13.-15. Oktober 1999, Essen, Publ. der DGPF, Vol. 8, Berlin.

- Diehl, H. and Heipke, C., 1992. Surface reconstruction from data of digital line cameras by means of object based image matching. In: ISPRS 17th Congress, Vol. IAPRS 29(B3) Comm. III, Washington, D.C., pp. 287–294.
- Englisch, A. and Heipke, C., 1998. Erfassung und Aktualisierung topographischer Geo-Daten mit Hilfe analoger und digitaler Luftbilder. PFG 3, pp. 133–149.
- Haala, N., Stallmann, D. and Cramer, M., 1998. Calibration of directly measured position and attitude by aerotriangulation of three-line airborne imagery. In: ISPRS Comm. III Symposium 'Object Recognition and Scene Classification from Multispectral and Multisensor Pixels', Vol. IAPRS 32(3/1), Columbus, Ohio, pp. 23–30.
- Hofmann, O., Kaltenecker, A. and Müller, F., 1993. Das flugzeuggestützte, digitale Dreizeilenaufnahme- und Auswertesystem DPA – erste Erprobungsergebnisse. In: D. Fritsch and D. Hobbie (eds), Photogrammetric Week '93, Wichmann, Karlsruhe, pp. 97–107.
- Jacobsen, K., 1997. Self-calibration of IRS-1C PAN-camera. In: ISPRS Joint Workshop 'Sensors and Mapping from Space', Hannover, pp. 163–170.
- Kaiser, B., Schmolla, M. and Wrobel, B. P., 1992. Application of image pyramid for surface reconstruction with FAST Vision (=Facets Stereo Vision). In: ISPRS 17th Congress, Vol. IAPRS 29(B3) Comm. III, Washington, D.C., pp. 341–345.
- Kornus, W., Lehner, M. and Schroeder, M., 1998. Geometric inflight calibration of the stereoscopic CCD-linescanner MOMS-2P. In: ISPRS Comm. I Symposium 'Earth Observation Systems for Sustainable Development', Bangalore, India.
- Lang, F. and Förstner, W., 1995. Matching techniques. In: W. Förstner and G. Ditzel (eds), Proc. of the Second Course in Digital Photogrammetry, Institut für Photogrammetrie, Universität Bonn.
- Meer, P., Baugher, E. S. and Rosenfeld, A., 1987. Frequency domain analysis and synthesis of image generating kernels. IEEE PAMI 9(4), pp. 512–522.
- Sandau, R., Fricker, P. and Walker, A. S., 1999. Digital photogrammetric cameras: possibilities and problems. In: D. Fritsch and R. H. Spiller (eds), Photogrammetric Week '99, Wichmann, Heidelberg, pp. 71–82.
- Schlüter, M., 1998. Multi-image matching in object space on the basis of a general 3-d surface model instead of common 2.5-d surface models and its application for urban scenes. In: ISPRS Comm. IV Symposium 'GIS – Between Visions and Applications', Vol. IAPRS 32(4), Stuttgart, pp. 545–552.
- Schlüter, M., 1999a. Geometrische Auswertung von DPA-Dreizeilenkameradaten. In: J. Albertz and S. Dech (eds), Photogrammetrie und Fernerkundung - Globale und lokale Perspektiven; Vorträge 18. Wissenschaftlich-Technische Jahrestagung der DGPF und 15. Nutzerseminar des Deutschen Fernerkundungsdatenzentrums, 14.-16. Oktober 1998, München, Publ. der DGPF, Vol. 7, Berlin, pp. 391–398.
- Schlüter, M., 1999b. Von der  $2\frac{1}{2}$ -D-zur 3D-Flächenmodellierung für die photogrammetrische Rekonstruktion im Objektraum. Dissertation, TU Darmstadt, DGK C 506, München.
- Schlüter, M., 2000. Fortführung von Geoinformationssystemen anhand direkt aufgezeichneter, digitaler Bilddaten. Mitteilungen des Bundesamtes für Kartographie und Geodäsie Bd. 14, Verlag des Bundesamtes für Kartographie und Geodäsie, Frankfurt am Main.
- Schlüter, M. and Kempa, M., 1993. DEM evaluation by an operator and Facets Stereo Vision: A comparison based on close-range imagery. In: A. Grün and H. Kahmen (eds), Optical 3-D Measurement Techniques II, Wichmann, Karlsruhe, pp. 502–509.
- Schlüter, M. and Wrobel, B. P., 1996. High resolution surface reconstruction of a landscape from large scale aerial imagery by Facets Stereo Vision – an extended test. In: ISPRS 18th Congress, Vol. IAPRS 31(B3) Comm. III, Wien, pp. 758–763.
- Tsay, J.-R., 1996. Wavelets für das Facetten-Stereosehen. Dissertation, TH Darmstadt, DGK C 454, München.
- Weisensee, M., 1992. Modelle und Algorithmen für das Facetten-Stereosehen. Dissertation, TH Darmstadt, DGK C 374, München.
- Wewel, F. and Brand, M., 1999. Geometrische Validierung des hochauflösenden multispektralen Mehrzeilenstereoscanners HRSC-A. In: J. Albertz and S. Dech (eds), Photogrammetrie und Fernerkundung - Globale und lokale Perspektiven; Vorträge 18. Wissenschaftlich-Technische Jahrestagung der DGPF und 15. Nutzerseminar des Deutschen Fernerkundungsdatenzentrums, 14.-16. Oktober 1998, München, Publ. der DGPF, Vol. 7, Berlin, pp. 245–252.
- Wrobel, B. P., 1987. Digital image matching by facets using object space models. In: Fourth International Symposium on Optical and Optoelectronic Applications in Science and Engineering 'Advances in Image Processing', SPIE, Vol. 804, The Hague, Niederlande, pp. 325–333.
- Wrobel, B. P., Kaiser, B. and Hausladen, J., 1992. Adaptive regularization of surface reconstruction by image inversion. In: W. Förstner and S. Ruwiedel (eds), Robust Computer Vision, Wichmann, Karlsruhe, pp. 351–371.